Solar Energy Materials & Solar Cells 161 (2017) 52–61

Contents lists available at ScienceDirect

Solar Energy Materials & Solar Cells

journal homepage: www.elsevier.com/locate/solmat

Polymer solar cells spray coated with non-halogenated solvents

Chaosheng Cai[a], Yangdong Zhang[a], Rongying Song[a], Zuosheng Peng[a], Lianpeng Xia[a], Mingxiao Wu[a], Kang Xiong[a], Biao Wang[a], Yuanbao Lin[a], Xiaofeng Xu[b], Quanbing Liang[c], Hongbin Wu[c], Ergang Wang[b], Lintao Hou[a,*]

[a] Siyuan Laboratory, Guangzhou Key Laboratory of Vacuum Coating Technologies and New Energy Materials, Key Laboratory of Optoelectronic Information and Sensing Technologies of Guangdong Higher Education Institutes, Department of Physics, Jinan University, Guangzhou 510632, PR China
[b] Department of Chemistry and Chemical Engineering, Chalmers University of Technology, SE-412 96 Göteborg, Sweden
[c] Institute of Polymer Optoelectronic Materials & Devices, State Key Laboratory of Luminescent Materials & Devices, South China University of Technology, Guangzhou 510640, PR China

ARTICLE INFO

Keywords:
Polymer solar cells
Spray coating
Non-halogenated solvent
Transient solvent evaporation
Light trapping

ABSTRACT

Using spray-coating technique, we successfully fabricated conventional ITO-based and inverted ITO-free polymer solar cells (PSCs) based on a conjugated polymer poly[2,3-bis-(3-octyloxyphenyl) quinoxaline-5,8-diyl-*alt*-thiophene-2,5-diyl] (TQ1) as the donor and [6,6]-phenyl-C_{61}-butyric acid methyl ester ($PC_{61}BM$) or [6,6]-phenyl-C_{71}-butyric acid methyl ester ($PC_{71}BM$) as the acceptor. Environment-friendly non-halogenated solvents were used to process the active layers. The influence of substrate temperatures and processing solvents on the photovoltaic performance of the ITO-based TQ1:$PC_{61}BM$ PSCs was systemically investigated. A higher substrate temperature can accelerate the solvent evaporating rate and afford a micro-textured rougher surface, which efficiently reduced light reflectance and enhanced absorption. Furthermore, finer phase separation was observed when using this high substrate temperature, which led to enhanced photocurrent due to the reduced bimolecular recombination. The device performance of spray-processed PSCs using the non-halogenated solvent mixtures was comparable to that of spray-processed PSCs using the halogenated *o*-dichlorobenzene (*o*DCB), which demonstrates that the non-halogenated solvents are very promising in spray-processed PSCs. This work sheds new light on developing efficient roll-to-roll compatible spray-coated PSCs with environment-friendly solvents.

1. Introduction

In the past decade, polymer solar cells (PSCs) have attracted considerable attention due to their unique advantages of low cost, light weight, environmental benignity and flexibility through roll-to-roll (R2R) manufacturing [1–4]. Up to now, the power conversion efficiency (PCE) of above 11% has been achieved both for single junction [5,6] and tandem PSCs [7]. Such impressive performance promotes bulk heterojunction (BHJ) PSCs to be one of the most feasible and renewable energy techniques in future. As one of the widely used solution-processing technique, spin-coating is not suitable for the productive R2R fabrication of large-scale devices [2,8]. Towards large-scale module production, several new solution-processing techniques such as inkjet-coating [9], doctor blading [10] and screen printing [11], have gained growing interests now. Among these techniques, spray-coating [12,13] has recently been considered as a promising method with particular advantages such as less material loss, high production speed and various substrate compatibility, which has been successfully used to fabricate large-area PSCs [14,15].

Fabrication of large-scale PSCs involves the use of halogenated organic solvents, which has been banned worldwide due to the environmental and health hazards. Moreover, the use of halogenated solvents largely increases the overall production costs due to the specific requirement of personal protection and disposal of hazardous waste. Therefore, it is necessary to replace the toxic halogenated solvents with non-halogenated alternatives. However, halogenated solvents such as chloroform (CF), chlorobenzene (CB) and *o*-dichlorobenzene (*o*DCB), usually afford higher device performance in PSCs. Recent study reveals that some of non-halogenated solvents such as toluene (TL), xylene and trimethylbenzene can attain comparable device performance. The key limiting factor is the poor solubility of fullerene derivatives in non-halogenated solvents. This leads to large fullerene aggregates and large-scale phase segregation in the blend films, which significantly limits the device performance [16–18].

* Corresponding author.
E-mail address: thlt@jnu.edu.cn (L. Hou).

http://dx.doi.org/10.1016/j.solmat.2016.11.027
Received 5 May 2016; Received in revised form 21 September 2016; Accepted 23 November 2016

Therefore, it is essential to improve the solubility of fullerene in non-halogenated solvents. One facile method is using binary or ternary solvent mixtures to modulate the solubility of fullerene and polymer to achieve favorable donor/acceptor morphology [19,20]. For example, Park *et al.* used acetophenone and mesitylene mixtures instead of *o*DCB to fabricate spin-coated PSCs [21]. Chen *et al.* reported high-performance spin-coated PSCs using TL as the processing solvent and 2% 1-methylnaphthalene as the additive [20] or with various xylene mixtures as the processing solvents [22].

Using non-halogenated solvents, great progress has been achieved in spin-coating processed PSCs. However, the correlation between processing methods and device performance is not clear for spray-coating PSCs using non-halogenated solvents. Especially, the drying kinetics and charge decay dynamic of spray-processed blend films have not been systematically studied. In this work, we used an easily synthesized polymer poly[2,3-bis-(3-octyloxyphenyl)quinoxaline-5,8-diyl-*alt*-thiophene-2,5-diyl] (TQ1) as the donor, which afforded good efficiency of 6–7% in spin-coated PSCs with [6,6]-phenyl-C_{71}-butyric acid methyl ester ($PC_{71}BM$) as the acceptor [23,24]. Although spin-coated TQ1:[6,6]-phenyl-C_{61}-butyric acid methyl ester ($PC_{61}BM$) devices show low PCEs of 4–5% due to the weak $PC_{61}BM$ absorption-coefficient in visible region, the blends solution with $PC_{61}BM$ shows the more controllable surface tension and viscosity than with $PC_{71}BM$ [10,24], which are very important to inhibit the nozzle orifice blocking in production of large-area PSCs. Both spray-coating and spin-coating PSCs were fabricated using halogenated and non-halogenated solvents for comparison. The correlations between the drying kinetics and the photovoltaic parameters were investigated using different temperatures and processing solvents. It was noted that the TQ1:$PC_{61}BM$ PSCs spray-coated from the non-halogenated solvent mixture of TL: indane (ID) afforded analogous device performance compared to those using the halogenated *o*DCB (3.3% vs. 3.6%), which was also close to the PSCs using the spin-coating method (3.7%). The role of ID additive in TL is that it has a high boiling point and low vapor pressure with a good solubility of acceptors in conjunction with the non-halogenated property. It indicates that the non-halogenated solvent mixtures can replace the toxic *o*DCB in high-throughput spray-coating processed PSCs. In addition, since the production cost is another issue for commercialization of PSCs, we also study the spray-coated ITO-free inverted solar cells (IFISCs) using the solution-processed PEDOT:PSS as the anode and Al/TiO_x as the cathode, which is considered to be more useful for the R2R processing. The spray-coated and spin-coated IFISCs show comparable device performance. Using a higher substrate temperature in the spray-coated IFISCs, superior short-circuit current density (J_{sc}) of 7.30 mA/cm^2 and 8.27 mA/cm^2 was obtained in the TQ1:$PC_{61}BM$ and TQ1: $PC_{71}BM$ devices, respectively. Our approach presents a promising method to develop low-cost, large-scale environment-friendly PSCs using the spray-coating technique.

2. Experimental details

2.1. Materials

The molecular structures of TQ1, $PC_{61}BM$ and $PC_{71}BM$ are shown in Fig. 1a. $PC_{61}BM$ and $PC_{71}BM$ were purchased from Solenne. The TQ1 material was synthesized in our lab with the number-average molecular weight (M_n) of 71.0 kDa and a polydispersity index (PDI) of 3.7 [24]. All reagents and metals were purchased from Alfa, Dupont, GCRF, and used without further purification. The weight ratio of TQ1:$PC_{61}BM$ and TQ1:$PC_{71}BM$ used in this work is 1:2.5 (w/w). The non-halogenated TL:ID solvent mixtures and the halogenated *o*DCB are used as the processing solvent with the concentrations of 20 mg/mL and 40 mg/mL, respectively. For the non-halogenated TL:ID solvent mixtures, the active solutions were firstly prepared in the pure TL solvent and pure ID solvent respectively, and then the pure solutions based on the volume ratios were mixed. The boiling points

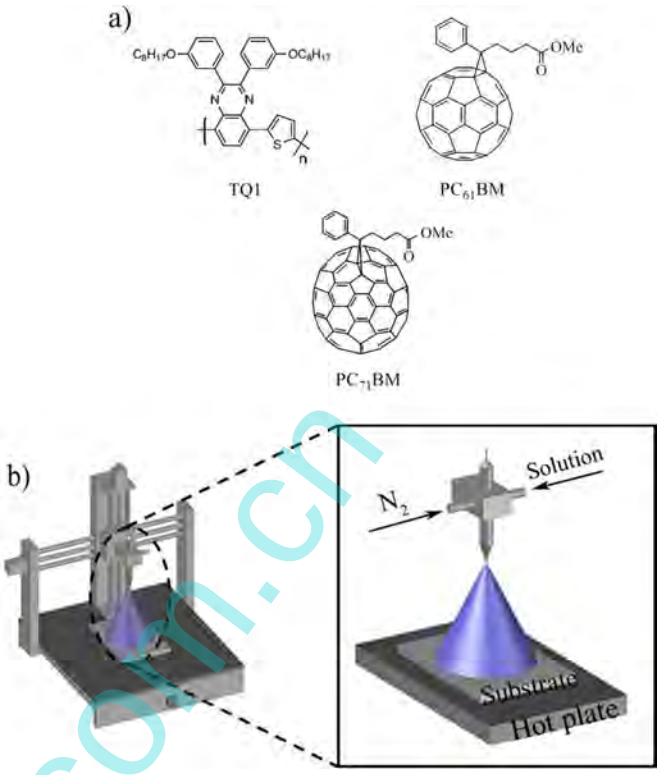

Fig. 1. (a) The molecular structures of TQ1, $PC_{61}BM$ and $PC_{71}BM$. (b) Setup of spray coating system with a zoom illustration.

of solvents were measured by Thiele tube. The vapor pressures of pure and mixed solvents were calculated by Antoine equation and Raoult's law (see details in Supplementary information (SI)). The thicknesses of the spray-coated films are controlled by changing the fabrication parameters, including the solution concentration and the spray-coating cycles [12,13,25].

2.2. Film characterization

Contact angles using water and formamide as the testing liquids were determined on solid active films prepared from different processing conditions using a drop shape analyzer DSA100 instrument (KRÜSS GmbH). These contact angles were converted into surface energy values based on the Owens method (see details in SI). To monitor the transient spray-coated wet film drying process, the film specular reflection excited by a blue LED was recorded by a CMOS camera (IDS uEye). The transient drying process of spin-coated wet films was achieved by synchronizing the camera with a near-infrared sensor, which was connected to a spin-coater. The thickness of final dry film was measured by a surface profilometer (XP-2). The film topography was investigated using atomic force microscope (AFM) (CSPM 5500), transmission electron microscopy (TEM) (JEM-2100F) as well as scanning electron microscopy (SEM) (ULTRA55, Zeiss). UV–vis absorption spectra were recorded on a Shimadzu UV-2550 UV–vis spectrophotometer.

2.3. Spraying process

The working principle of spray coating apparatus is described in Fig. 1b, which consists of four parts: The first part is the injection unit, which is composed of the 0.3 mm diameter nozzle orifice (MA-S), active solution and high-pressure nitrogen gas (N_2) for atomizing the solution. The second part is the heating unit to control the morphology of the spray-processed film. The third part is the moving unit, which

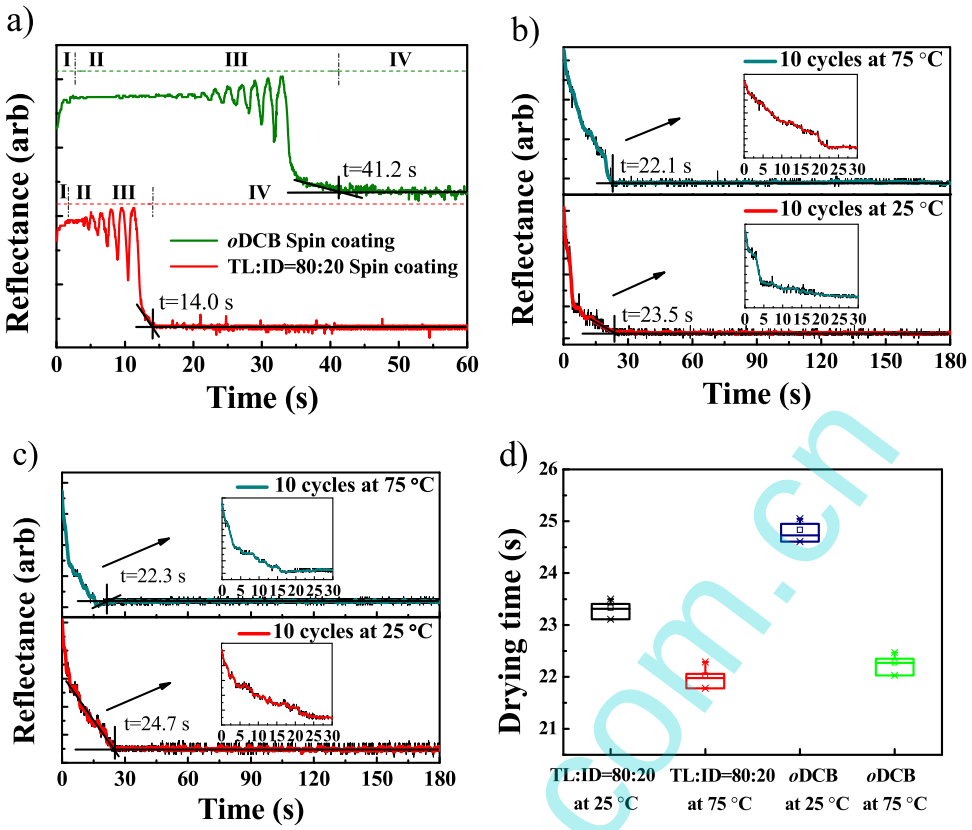

Fig. 2. The light reflectance versus time during the drying process of (a) the spin-coated TQ1:$PC_{61}BM$ film from TL:ID (80:20, v/v) (20 mg/mL) and *o*DCB (40 mg/mL) solvents at 1500 rpm, and the 10 cycles spray-coated TQ1:$PC_{61}BM$ films from (b) TL:ID (80:20, v/v) solvent mixtures and (c) *o*DCB solvent with the substrate temperature at 25 °C and 75 °C, respectively. Inset: a detailed enlarged view of the reflectance image. (d) Statistical drying time of the spray-coated films processed from TL:ID (80:20, v/v) and *o*DCB solvents at 25 °C and 75 °C. The horizontal lines in the box denote the 25th, 50th and 75th percentile values, and the error bars denote the 5th and 95th percentile values with the mean values denoted by the open square inside the box.

pushes the nozzle orifice to be moved in any desired direction. The last part is the control unit, which is used to tune the moving unit speed, spraying route and range, and heating temperature for a precise adjustment of the film quality in a wide substrate range. In this experiment, the nozzle orifice followed the moving unit at a constant speed of 60 cm/min when spray coating was working under way. The active layer thickness was controlled by increasing the spraying cycles from 1 to 10.

A minimum N_2 pressure is necessary to allow the atomization of the active solution and a high N_2 pressure decreases the size of the droplets to form a more regular film. However, if the N_2 pressure is too high, the droplets will be blown away once they hit the substrate, leading to a lot of cracks in the resulting film. Furthermore, a short nozzle-to-substrate distance leads to de-wetting occurrence, whereas a long distance results in a dry and dusty film [26]. In this experiment, an ideal nozzle-to-substrate distance of 15 cm with a N_2 pressure of 0.3 MPa was empirically determined. The property of the processing solvents plays an important role in the selection of suitable liquid flow rate which is controlled by the N_2 gas flow rate (2.5 l/min) for spray-coating technique. For the relatively volatile solvent TL:ID, a high liquid flow rate (0.8 mL/min) was required during the spraying process in order to obtain much evener surface topography with combined droplets on the substrate, whereas for a high boiling point solvent *o*DCB, a low liquid flow rate (0.6 mL/min) was adopted [27].

2.4. Device fabrication and characterization

The conventional PSCs were fabricated with a configuration of glass/ITO/PEDOT:PSS/active layer/LiF/Al, as shown in Fig. S1a. The ITO-coated glass substrates were ultrasonically cleaned with acetone, detergent, de-ionized water and isopropanol in turn, followed by an oxygen plasma treatment for 120 s for further cleaning and improving the work function of ITO. As a buffer layer, the conductive polymer PEDOT:PSS (Baytron PVP Al 4083) was spin coated at 3500 rpm for 60 s (approximately 40 nm) onto ITO-coated glass substrates, and annealed at 120 °C for 10 min. The active layer was spray-coated or spin-coated at 1500 rpm in ambient atmosphere with the same solution formulation, making the process transfer from spin coating to spraying coating more simple and rational. LiF (0.6 nm) and Al (100 nm) as the top electrode were deposited onto the active layer in vacuum. For IFISCs (as shown in Fig. S1b), Al (80 nm) and Ti (4 nm) as the bottom electrode were thermally evaporated onto the glass substrate through a shadow mask and exposed to air for 12 h to form TiO_x. A conjugated interfacial modification polymer poly[(9,9-bis(3′-(N,N-dimethylamino) propyl)-2,7-fluorene)-*alt*-2,7-(9,9-dioctylfluorene)] (PFN) was synthesized in our group and was spin coated on top of the TiO_x surface with a concentration of 0.2 mg/mL in methanol at 2000 rpm for 60 s. The PEDOT:PSS PH1000 (Clevious) solution mixed with 5% dimethyl sulfoxide (DMSO) and 0.5% surfactant (FS 300, Zonyl) was spin-coated on top of the active layer at 1500 rpm for 60 s followed by annealing at 70 °C for 30 s. All the devices have the active area of 14 mm^2. For verifying the large-scale spray coating method effectiveness, the devices with the active area of 1 cm^2 were also made.

The current-density-voltage (*J–V*) characteristic measurements were recorded with Keithley 2400 source under AM 1.5 G illumination (100 mW/cm^2) of a solar simulator (Sun 2000, Abet). The light intensity of the solar simulator was calibrated by a standard silicon photodiode. The external quantum efficiency (EQE) data were measured by a QE-R test system from Enli technology company (Taiwan).

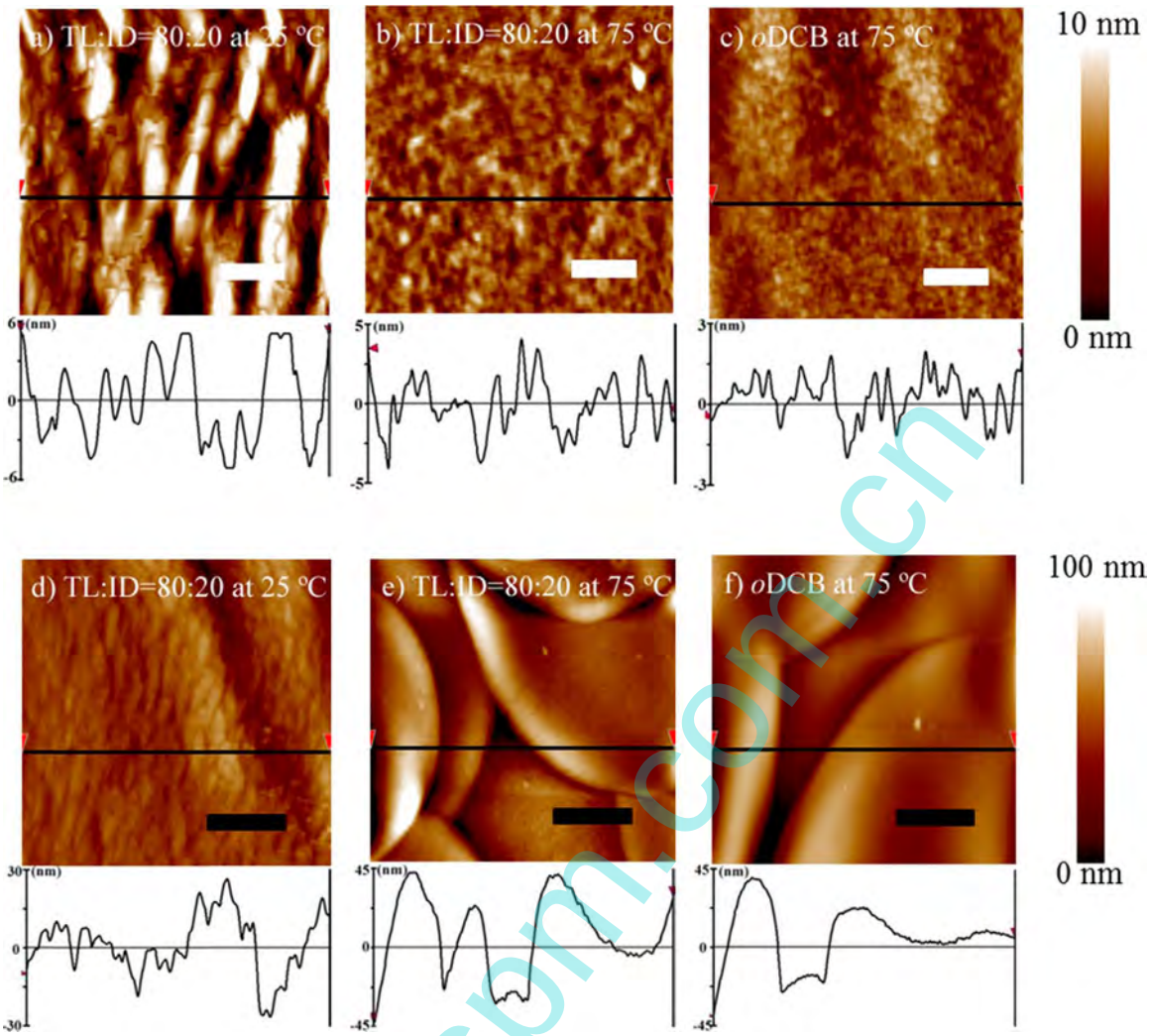

Fig. 3. Tapping mode AFM images (a, b and c: 5 μm×5 μm; d, e and f: 16 μm×16 μm) of spray-coated TQ1:$PC_{61}BM$ films with the substrate temperature at 25 °C (a, d) and 75 °C (b, e) using the non-halogenated TL:ID (80:20, v/v) as the solvent in comparison with the TQ1:$PC_{61}BM$ film using the halogenated *o*DCB as the solvent at substrate temperature of 75 °C (c, f). The white scale bars represent 1 μm while the black scale bars represent 4 μm.

Transient photovoltage (TPV) measurement was performed under the open-circuit condition and an illumination of a 100 W tungsten halogen lamp. The devices were connected to an oscilloscope (Tektronix DPO4104, 1 GHz) with an input impedance of 1 MΩ to hold the device at the open-circuit condition. The excitation pulse was generated using a pulsed laser with a wavelength of 532 nm (OPOTEK Vibrant 355, with a 5 ns optical pulse). The perturbation light intensity was attenuated by a set of neutral density filters so that the amplitude of TPV is much less than V_{oc}. Transient photocurrent (TPC) measurement was performed with the device being held under a short-circuit condition by connecting the device to the ground through a small resistor. The resulting transient current was measured using an oscilloscope in parallel with a small resistor of 25 Ω. The excitation pulse was generated using a pulsed laser.

3. Results and discussion

3.1. Transient film formation process

The film morphology is formed during the drying process, which is significantly affected by the rate of solvent evaporation. Here, we applied a transient in situ monitoring technique to study the different drying processes of the two film-forming methods. Fig. 2a-c exhibits the transient film formation processes of the spin-coated and spray-coated wet films from non-halogenated TL:ID (80:20, v/v) and halogenated *o*DCB solvents. The film drying processes of spin-coating and spray-coating are quite different. Four different stages are identified during the spin-coated drying process of the wet films, as shown in Fig. 2a. At the initial stage of spin-coating (stage I), a fast increase of the reflectance spectrum appears due to the large loss of the wet material. After several seconds, the constant intensity of the reflected spectrum is observed (stage II), indicating the wet film no longer loses. However, the film is still too thick to generate any detectable interference fringes. With the durative solvent evaporation, a high interference oscillation frequency occurs (stage III), which means the solvent is rapidly evaporated. The last constant intensity reflectance spectrum indicates the active layer is thoroughly dried (stage IV). It is noted that the non-halogenated solvent mixtures have a much shorter evaporation time than that of the halogenated solvent. Unlike the drying process of spin-processed wet films, only two stages are identified during the drying process of the ten cycles spray-processed wet films as presented in Fig. 2b-c. The reflectance of the wet films decreases rapidly with the undetectable interference fringes due to the rapid solvent evaporation. For the non-halogenated solvent mixtures, the spray drying time which is determined by the intersection of the tangent curve and the straight line is 23.5 s and 22.1 s at 25 °C and 75 °C, respectively. However, for the halogenated solvent, the spray drying time increases to 24.7 s and 22.3 s, respectively. The speed of

the solvent volatilization is faster when the temperature is higher for spray-coated films. The little difference in drying time for the two solutions at 75 °C implies that the spray-coated droplets are very tiny and easy to be solidified. Fig. 2d shows the statistical drying time diagram of the spray-coated films processed from non-halogenated and halogenated solvents at 25 °C and 75 °C. The average final drying time is approximately 23.4 s and 22.1 s for the films sprayed at 25 °C and 75 °C respectively using the non-halogenated TL:ID (80:20, v/v) as the solvent, while the corresponding average drying time is 24.8 s and 22.3 s for the films processed from the halogenated *o*DCB as the solvent, respectively. It was noted that the drying time at the whole substrate for the two types of solvents are similar, demonstrating that spray coating is a promising method to form uniform films by tuning the spraying speed and route. To further investigate the temperature effect on the drying process, the drying time of the one-cycle atomized droplets was measured at different substrate temperatures, as shown in Fig. S2a-b. It is observed that the drying time becomes shorter with the increase of substrate temperature, indicating a faster drying rate in the higher substrate temperature. The result of the one cycle spraying process is consistent with that of the above ten cycles spraying process.

3.2. Film morphology

The surface topographies of the active layers measured via AFM are shown in Fig. 3. The detailed roughness distribution of the spray-processed film along the black horizontal line is also given, which clearly exhibits the detailed vertical height difference of the film surface. The spray-processed photoactive layer using the non-halogenated TL:ID (80:20, v/v) solvent mixtures at 25 °C yields a root mean square (RMS) roughness of 2.96 nm in a small area (5 μm×5 μm) (Fig. 3a), whereas it becomes 10.6 nm in a large area (16 μm×16 μm) (Fig. 3d) due to the droplet merging and overlapping. As observed in Fig. 3b, the size of the donor/acceptor phase separation of the TL:ID spray-processed film decreases at 75 °C, which is consistent with its reduced RMS roughness of 1.33 nm compared to 2.96 nm at 25 °C. Similarly, the RMS value in a large area becomes higher (18.4 nm) due to the faster solvent evaporation of multiple overlapping ring-structure domains, as shown in Fig. 3e. The results suggest that a relatively high substrate temperature can contribute to form a finer nanostructure and a rougher microstructure by accelerating the drying rate of the droplets and reducing the miscibility among the droplets. In addition, the photoactive film sprayed from the halogenated *o*DCB at 75 °C shows the RMS value of 1.23 nm in a small area and 9.80 nm in a large area respectively, as presented in Fig. 3c and f, which tendency is identical to the results of the film processed from the non-halogenated TL:ID (80:20, v/v) solvent mixtures at 75 °C. The higher RMS value of the photoactive film from non-halogenated solvent mixtures than that from the halogenated *o*DCB at 75 °C (18.4 vs. 9.80 nm) in a large area (16 μm×16 μm) is due to the faster non-halogenated solvent mixtures evaporation in ring-structure multi-droplets.

Fig. 4a-c shows the corresponding SEM images of the randomly aligned spray-coated photoactive films at different conditions. It is noted that the substrate temperature has an important impact on the droplet size and shape. The size of the majority of atomized TQ1:$PC_{61}BM$ droplets from the non-halogenated TL:ID (80:20, v/v) in SEM images decreases when the processing temperature increases from 25 °C to 75 °C due to a faster drying rate of the droplets, which is also consistent with the difference of RMS values between 25 °C and 75 °C in a large area. The ring-like stain shapes with the well-known “coffee-stain” effect were observed for the atomized droplet deposited at 25 °C, which is eliminated by improving the substrate temperature to 75 °C due to the counterbalance by convective flow and Marangoni flow [28]. The spray-coated film from the halogenated *o*DCB solvent at 75 °C shows the similar morphology to that from the non-halogenated TL:ID (80:20, v/v) at 75 °C. Besides the SEM images, the eliminating “coffee-stain” effect at higher temperature is also proved by the individual atomized droplet surface profiles (Fig. 4e-f).

The observed variation in surface morphology by AFM and SEM is correlated with a series of the 3D nanostructures of the spray-coated blends. In Fig. 5, the internal morphological structures of spray-coated TQ1:$PC_{61}BM$ films were characterized using TEM images with the associated selective area diffraction (SAD) patterns. As shown in Fig. 5a-b, the bulk size of the atomized droplets decreases when the processing temperature increases from 25 °C to 75 °C for the TQ1:$PC_{61}BM$ films using the non-halogenated TL:ID (80:20, v/v) solvent mixtures, which is consistent with SEM images of the corresponding film surface (Fig. 4). The spray-coated film from the halogenated *o*DCB at 75 °C (Fig. 5c) shows a larger droplet size than that from TL:ID (80:20, v/v) solvent mixtures at 75 °C due to its higher solvent boiling point, which makes spray-coated droplets spread over the substrate surface to a large extent and be dried to a solid film for a longer time (Fig. 2). As shown in Fig. 5d-f, the high-resolution TEM image of the spray-casted TQ1:$PC_{61}BM$ films at 25 °C from the non-halogenated TL:ID (80:20, v/v) solvent mixtures displays big domains

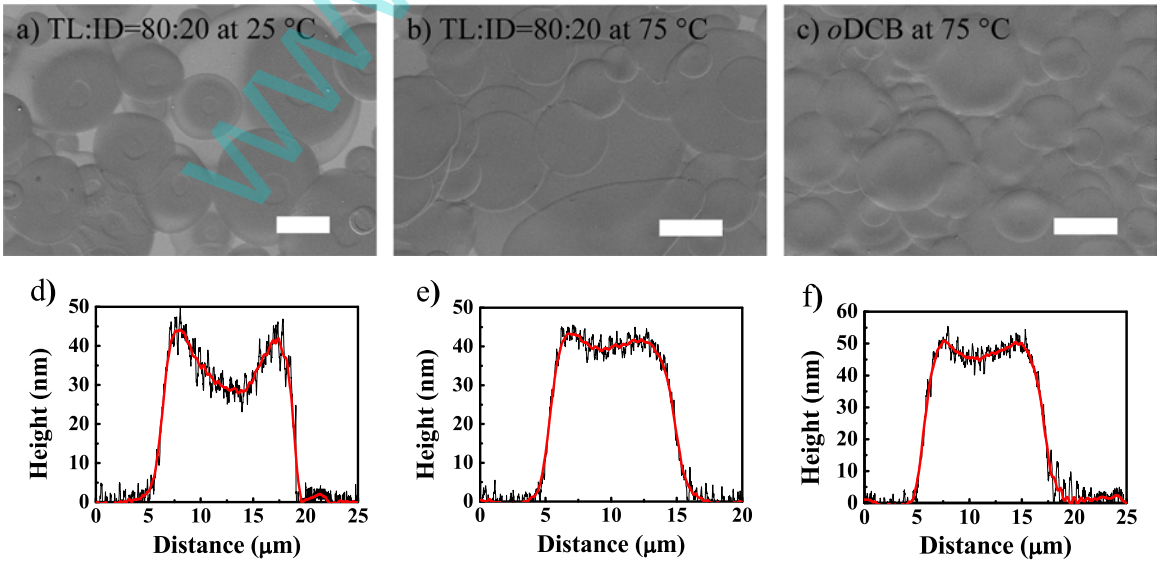

Fig. 4. Surface SEM images (top) and individual atomized droplet surface profiles (bottom) of the spray-coated TQ1:$PC_{61}BM$ films processed from TL:ID (80:20, v/v) with the substrate temperature (a, d) at 25 °C and (b, e) at 75 °C, as well as from *o*DCB (c, f) at 75 °C. The white scale bars represent 20 μm.

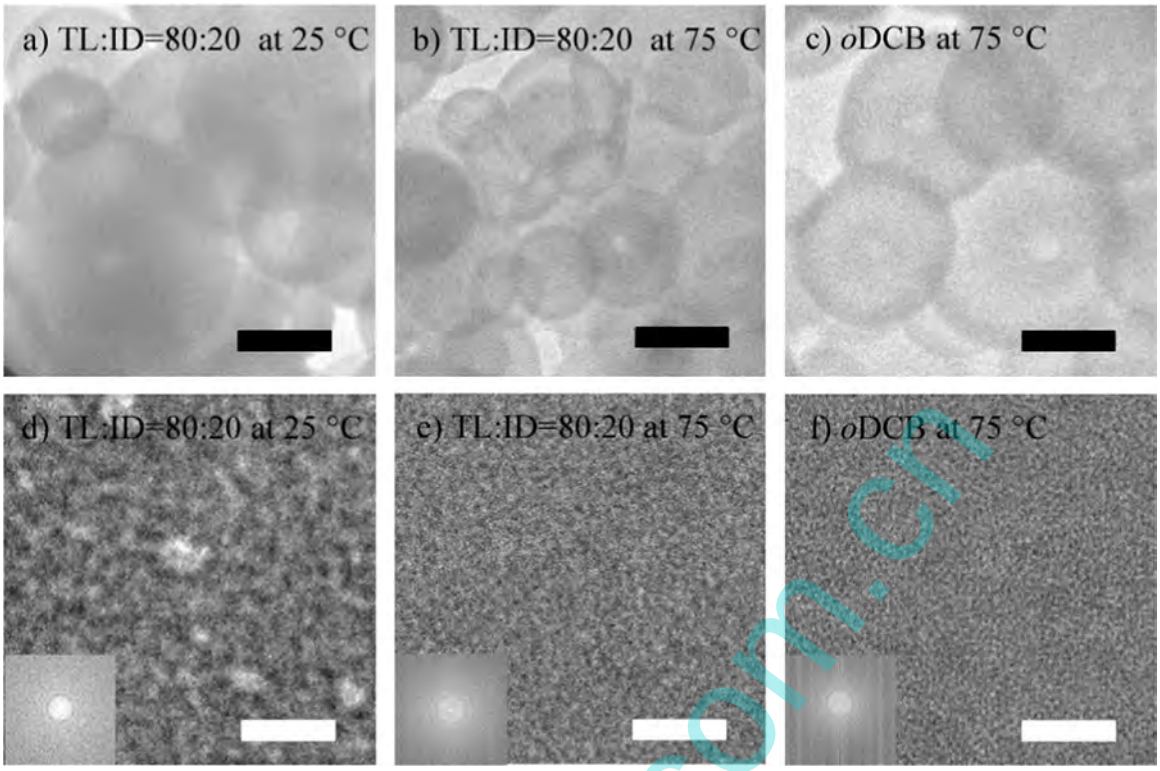

Fig. 5. TEM micrographs of TQ1:$PC_{61}BM$ composite films fabricated by spray coating from the non-halogenated TL:ID (80:20, v/v) solvent mixtures with the substrate temperature (a, d) at 25 °C and (b, e) at 75 °C, as well as from the halogenated *o*DCB solvent (c, f) at 75 °C. The black scale bars represent 10 μm while the white scale bars represent 50 nm.

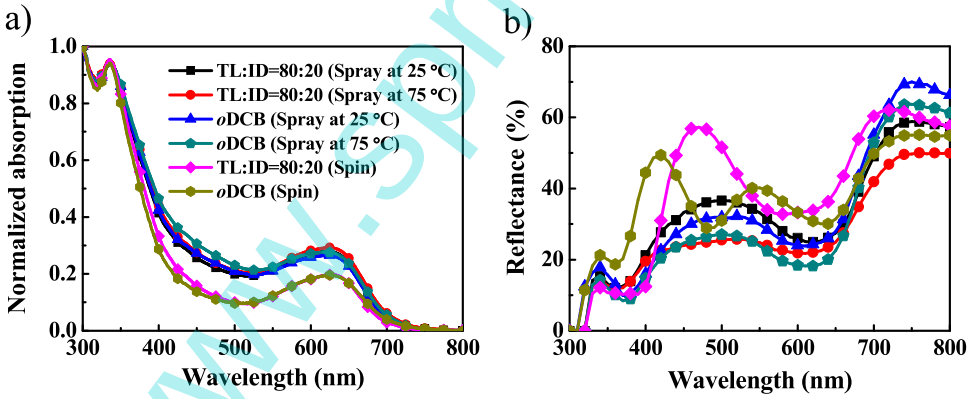

Fig. 6. (a) Normalized UV–vis absorption spectra of TQ1:$PC_{61}BM$ films processed with various film-forming methods and solvent compositions. (b) Reflectance of the corresponding PSCs with the structure of ITO/PEDOT:PSS/active layer/LiF/Al.

where the light and dark features were assigned to the aggregations of the polymer and $PC_{61}BM$, respectively [23]. However, much smaller donor/acceptor domain sizes were observed for the films formed from the non-halogenated TL:ID (80:20, v/v) solvent mixtures or the halogenated *o*DCB solvent at 75 °C. Moreover, brightly and clearly distinguished diffraction rings were also discovered in SAD for the films sprayed at 75 °C. However, no such diffraction feature was found in Fig. 5d, which suggests the π-π stacking of the TQ1:$PC_{61}BM$ blends increases with the increase of the substrate temperature from 25 °C to 75 °C [23].

For further exploring the surface components of the BHJ films, surface energies of spray-coated BHJ solid films were measured using water and formamide as the probe liquids based on Owens equation $\gamma_l(1+\cos\theta)=2(\gamma_s^D\gamma_l^D)^{1/2}+2(\gamma_s^P\gamma_l^P)^{1/2}$, where γ_s and γ_l are the surface energies of the sample and the probe liquid, and D and P refer to the dispersion and polar components of the surface energy, respectively (see details in the SI). As displayed in Fig. S3, the surface energies of the spray-coated BHJ films processed from both halogenated *o*DCB solvent (22.5 ± 0.2 mN/m) and non-halogenated TL:ID (80:20, v/v) binary solvent mixtures (24.2 ± 0.4 mN/m) are similar to that of pure TQ1 (21.04 mN/m) but much lower than that of pure $PC_{61}BM$ (36.67 mN/m), which suggests that the spray-processed top surface is richer in TQ1. Furthermore, the higher surface energy of the spray-coated BHJ film processed from the non-halogenated TL:ID (80:20, v/v) indicates that more $PC_{61}BM$ molecules are on top of the TQ1:$PC_{61}BM$ film surface compared with that from the halogenated *o*DCB solvent, which is advantageous to facilitate the electron collection for the non-halogenated spray-coated conventional device (ITO/PEDOT:PSS/active layer/LiF/Al) [29,30].

3.3. Absorption and reflectance

It is worth noting that substrate annealing temperature has considerable effect on the film absorption due to the reorganization of polymer ordering [31,32]. In fact, the film absorption is also influenced by the different film-forming methods as well as the different solvents [10,33,34]. Fig. 6a shows the absorption spectra of spin-coated and spray-coated TQ1:$PC_{61}BM$ films processed from the halogenated *o*DCB and the non-halogenated TL:ID (80:20, v/v) solvent mixtures. A main difference between spin-coated and spray-coated films is that the absorption from 350 to 720 nm is significantly enhanced for spray-processed films no matter which solvent was used. This is mainly attributed to the light trapping by the randomly textured surfaces of the films possessed by spray coating (Figs. 3–5). Thus it can be seen that spray coating provides a simple and efficient route to increase the light absorption. Moreover, compared to spray-coated films processed at 25 °C, a slight increase in the absorption was observed for spray-coated films processed at 75 °C, corresponding to the higher RMS roughness.

To further study the enhanced light absorption of spray-coated films, the reflectance spectra of the corresponding devices were investigated, as shown in Fig. 6b. The reflectance intensity of spin-processed devices is much stronger than that of spray-processed devices in a wide wavelength range from 300 to 650 nm, indicating that light absorption is less in spin-coated PSCs. It can be speculated from the rough microstructure of the spray-processed surface that the incident solar light was scattered and thus the light path length in the active layer was increased, leading to the increase of light harvesting and decrease of light reflectance. Furthermore, with the increase of the substrate temperature, the reflectance intensity of spray-processed devices processed from two types of solvents decreases in a wide wavelength range from 300 to 800 nm. The concrete reflectance spectra of non-halogenated TL:ID (80:20, v/v) spray-processed devices in different temperatures are shown in Fig. S4. The reduced reflectance with the increase of the substrate temperature is consistent with the morphology measurements that a higher substrate temperature aids to form a rougher microstructure, leading to more photons absorption in the active layer.

3.4. Charge transport property

To get more insight into correlations between solvent properties and film-forming conditions on charge transport in spray-processed PSCs, the hole and electron mobilities of the TQ1:$PC_{61}BM$ active layers were measured using the space-charge-limited current (SCLC) model. The electron mobility was measured with an electron-transport-only device configuration of ITO/Al(10 nm)/LiF(0.6 nm)/TQ1:$PC_{61}BM$(110 nm)/LiF(0.6 nm)/Al(100 nm), and the hole mobility with a hole-transport-only device structure of ITO/MoO_3(10 nm)/TQ1:$PC_{61}BM$(110 nm)/MoO_3(10 nm)/Al(100 nm). As presented in Fig. 7a, the hole and electron mobilities of non-halogenated TL:ID spray-coated active layers are comparable to those of halogenated *o*DCB spray-coated films at 75 °C, which is consistent to their similar nanostructure morphologies in blend films. The hole mobility of non-halogenated TL:ID spray-coated active layer at 75 °C is one order of magnitude higher than that of active layer sprayed at 25 °C, while the electron mobility is nearly invariable with the increase of substrate temperature. This is in agreement with previous reports about the charge mobility enhancement through thermal annealing for spin-coated PSCs [35]. To further shed light on how the processing temperature influences the charge transport and collection in devices, we performed TPV and TPC measurements to probe the charge decay dynamics and charge density in halogenated and non-halogenated spray-coated TQ1:$PC_{61}BM$ devices with the substrate temperature at 25 °C and 75 °C [36–40]. Since there is no charge collected under open-circuit voltage (V_{oc}) condition, the excess charge carriers excited

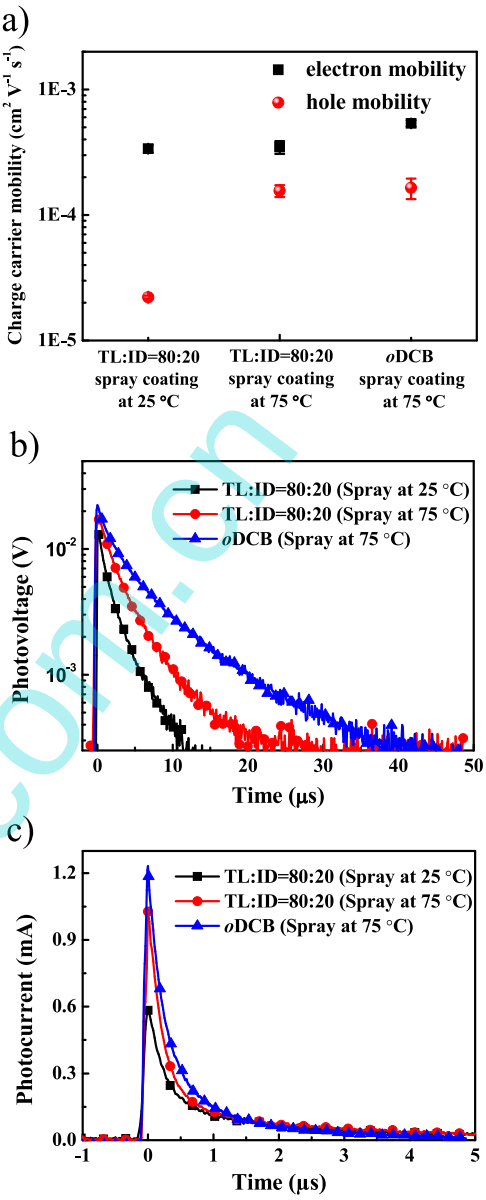

Fig. 7. (a) The charge carrier mobilities of spray-coated TQ1:$PC_{61}BM$ films with the different solvents as well as substrate temperatures. Error bar represents the standard deviation of 10 individual devices. (b) TPV of the corresponding spray-coated TQ1:$PC_{61}BM$ PSCs measured under 1 sun illumination and V_{oc} conditions and (c) TPC measured under a short-circuit condition using the same intensity laser pulse.

by the pulsed laser are recombined and their lifetime can be extracted from the exponential fitting on the decay of the TPV. Fig. 7b shows the TPV measurement results of spray-coated TQ1:$PC_{61}BM$ devices with the substrate temperature at 25 °C and 75 °C using non-halogenated TL:ID (80:20, v/v) solvent mixtures. The extracted carrier lifetimes are 1.81 μs and 3.0 μs for spray-coated TQ1:$PC_{61}BM$ devices with the substrate temperature at 25 °C and 75 °C, respectively. For comparison, the lifetime of the TQ1:$PC_{61}BM$ device using halogenated *o*DCB at 75 °C is 4.88 μs. The observed longer carrier lifetime of devices at a higher substrate temperature suggests the bimolecular recombination is significantly reduced, which is advantageous to improve the device performance [41]. The longer carrier lifetime for *o*DCB spray-coated devices than TL:ID at 75 °C (4.88 μs vs. 3.01 μs) is mainly due to the better film morphology, which effectively promotes exciton separation and carrier generation (Figs. 3 & 5). Moreover, as revealed by the TPC curves (Fig. 7c), the devices at 75 °C show a higher charge carrier

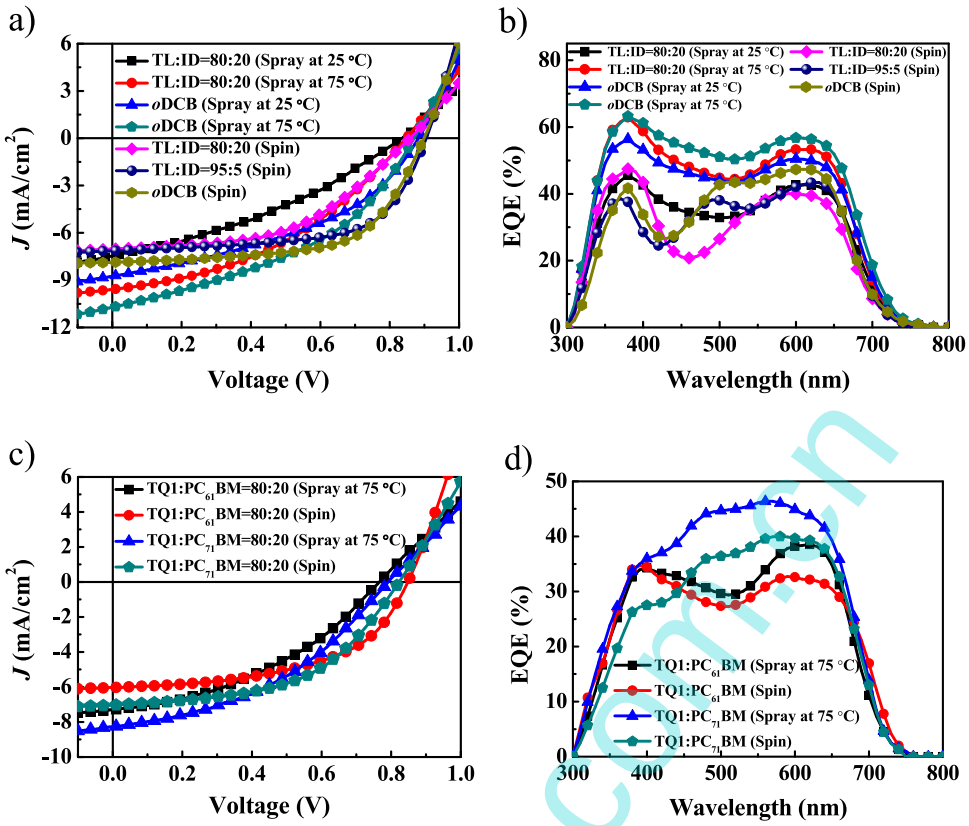

Fig. 8. (a) *J–V* characteristics and (b) the corresponding EQE spectra of conventional structure TQ1:PC_{61}BM PSCs based on spin coating and spray coating with different solvents and substrate temperatures. (c) *J–V* characteristics and (d) the corresponding EQE spectra of the TQ1:PC_{61}BM and TQ1:PC_{71}BM IFISCs based on spin coating and spray coating (75 °C) using non-halogenated TL:ID (80:20, v/v) solvent mixtures.

density compared to that at 25 °C, which agrees with the TPV measurements. Thus it can be concluded that the improved charge transport characteristics at higher temperature will definitely result in the enhancement of the PSC performance.

3.5. Device photovoltaic performance

The substrate temperature plays a fundamental role in dominating the nano/micro-scale morphology and charge transport property of the active layers by controlling the drying time of the wet films for both halogenated and non-halogenated solvents. Fig. 8a presents the *J–V* characteristics of TQ1:PC_{61}BM PSCs by spray coating and spin coating with the structure of ITO/PEDOT:PSS/active layer/LiF/Al. The devices spray-coated at 75 °C exhibit better photovoltaic performance compared with those spray-coated at 25 °C for both halogenated and non-halogenated solvents. An average 80% improvement of PCE for TQ1:PC_{61}BM devices spray-processed from TL:ID (80:20, v/v) solvent mixtures has been achieved with the increase of temperature from 25 to 75 °C, whereas only an average 12% improvement of PCE for TQ1:PC_{61}BM devices spray-processed from the halogenated *o*DCB solvent under a similar condition. The improvement is mainly due to the increase of J_{sc}. The larger PCE increase for devices from the non-halogenated TL:ID (80:20, v/v) solvent mixtures is mainly due to the finer morphology of the active layers with less phase separation and more light scattering at higher temperature (as illustrated in Figs. 3–6). The reduced fill factor (FF) and V_{oc} of all spray-coated devices are correlated with the numerous pinholes and larger donor/acceptor phase separation compared to that of spin-coated devices [24,32]. The concrete device performance parameters are summarized in Table 1. The corresponding EQE spectra of spray-coated TQ1:PC_{61}BM PSCs are presented in Fig. 8b. The devices processed from non-halogenated and halogenated solvents at 75 °C show the higher EQE intensity compared to that of the spin-coated devices. Moreover, for the spray-coated device processed from halogenated *o*DCB solvent at 25 °C, the EQE response is stronger than that of the corresponding spin-coated device. The enhanced photoresponse in spray-coated devices is mainly attributed to the efficient light harvesting and trapping, as indicated by the weak reflectance spectra (Fig. 6b).

For seeking the optimal annealing temperature, four different high substrate temperatures (55, 65, 75 and 85 °C) were used for non-halogenated TL:ID TQ1:PC_{61}BM devices. As shown in Fig. S5a and Table S2, the device performance increases with increasing substrate temperature from 55 to 75 °C and then decreases at 85 °C. The lower PCE of the device deposited at 85 °C than that at 75 °C is likely due to the increased droplet-droplet interface density which would resist the charge flow [42,43]. The EQE curves of the spray-coated devices at various substrate temperatures show the same shape in the entire range of wavelength (Fig. S5b). The maximum EQE value of the device spray-coated at 25 °C is 46%, which gradually increased to 51%, 58%, 65% and 57% when increasing the substrate temperature from 55 to 85 °C, respectively. The maximum EQE of 65% is one of the highest values among the TQ1:PC_{60}BM PSCs [23]. The photocurrents calculated via integrating the EQE are coherent with those obtained from the *J–V* measurements (within 4% error). The "false" internal quantum efficiency (FIQE) of the PSCs spray-coated at different substrate temperatures was calculated based on the reflectance spectrum and EQE curve if the parasitic absorptions of non-photoactive layers related to the ITO, PEDOT:PSS and LiF/Al were ignored. The FIQE of the spin-coated PSCs was also carried out. As shown in Fig. S5c, it is found that the device spray-coated at 75 °C exhibits higher FIQE intensity than those spray-coated at 25, 55, 65, 85 °C and that spin-coated at 25 °C. Secondly, the film thickness is another key parameter for determining the devices performance. As exhibited in Fig. S6, the non-halogenated TL:ID PSCs with 120 nm thick spray-coated active

Table 1
Photovoltaic parameters of the devices fabricated under various conditions. Over 10 individual devices were measured for each averaged value.

Method	Solvent	T[d] (°C)	Thickness (nm)	J_{sc} (mA/cm^2)	V_{oc} (V)	FF	Highest PCE (%)	Average PCE (%)
Spray[a]	TL:ID=80:20	25	120	7.47	0.83	0.35	2.1	1.8
Spray[a]	TL:ID=80:20	75	120	9.72	0.85	0.40	3.3	3.3
Spray[a]	*o*DCB	25	110	9.14	0.88	0.40.	3.2	3.2
Spray[a]	*o*DCB	75	110	10.76	0.87	0.42	3.9	3.6
Spray[a]	TL:ID=95:5	75	110	3.40	0.86	0.24	0.7	0.6
Spin[a]	TL:ID=95:5	25	110	7.14	0.91	0.63	4.1	3.7
Spin[a]	TL:ID=80:20	25	110	7.03	0.86	0.49	3.0	2.6
Spin[a]	*o*DCB	25	115	7.83	0.90	0.61	4.4	4.1
Spray[b]	TL:ID=80:20	75	110	7.30	0.77	0.40	2.2	2.1
Spin[b]	TL:ID=80:20	25	110	6.03	0.83	0.53	2.6	2.4
Spray[c]	TL:ID=80:20	75	110	8.27	0.79	0.41	2.7	2.4
Spin[c]	TL:ID=80:20	25	110	7.04	0.82	0.52	3.0	2.8

[a] ITO/PEDOT:PSS/TQ1:$PC_{61}BM$/LiF/Al.
[b] Al/TiO_x/PFN/TQ1:$PC_{61}BM$/PEDOT:PSS.
[c] Al/TiO_x/PFN/TQ1:$PC_{71}BM$/PEDOT:PSS.
[d] Substrate temperature.

films can obtain the comparable device performance to that of the halogenated *o*DCB spray-coated PSCs with 110 nm thick spray-coated active films (3.3% vs. 3.6%). However, the non-halogenated TL:ID spray-processed device performance decreases with the increase of active film thickness, which is different from that of the *o*DCB halogenated spray-coated PSCs. We speculate that the droplet-droplet interface has a larger influence on the TL:ID device performance compared to the halogenated device performance, which can be seen from the decreased FF with the increase of active film thickness. Thirdly, the volume ratio of ID in non-halogenated solvent mixtures also has a big impact on spin-/spray-coated device performance. As shown in Fig. S7, the optimal ID concentration is 5% (v/v) for non-halogenated TL:ID spin-coated devices whereas it is 20% (v/v) for spray-coated devices, implying that the transfer of different coating methods using binary non-halogenated solvent mixtures is not so simple since the different evaporation process requires the different ID doping ratios for attaining the optimal film morphology. The corresponding experimentally measured boiling point and calculated vapor pressure of TL:ID (95:5, 90:10, 85:15 and 80:20, v/v) solvent mixtures are shown in Table S3 compared to pure solvents. The TL:ID (80:20, v/v) has the highest boiling point (129 °C) and lowest vapor pressure (2.99 KPa@25 °C, 57.69 KPa@98 °C) in mixed solvent mixtures, which endows the sprayed droplets with a good morphology control. For validating the spray-coating method in large-scale manufacturing, Fig. S8 plots the white-dark *J*–*V* and EQE curves of spray-coated devices with an area of 1 cm^2 using halogenated and non-halogenated solvents at 75 °C. The spray-coated PSCs fabricated using TL:ID can achieve a comparable PCE compared with those fabricated using *o*DCB (1.4% vs. 1.5%), indicating the environment-friendly solvent effectiveness in large-area spraying wet processing. The lower PCE values of 1 cm^2 area may mainly come from the larger ITO resistance as compared to small area (14 mm^2) (Table S4).

Since there is no report on spray-coated and ITO-free PSCs using non-halogenated solvents, we also fabricated spray-coated IFISCs (Al/TiO_x/PFN/active layer/PEDOT:PSS) using the non-halogenated solvent mixture. The *J*–*V* characteristics of the IFISCs prepared by spin/spray coating are presented in Fig. 8c. Average PCEs up to 2.1% and 2.4% were observed for spray-coated IFISCs based on TQ1:$PC_{61}BM$ and TQ1:$PC_{71}BM$, respectively, in comparison with average PCEs of 2.4% and 2.8% of the corresponding spin-coated devices. It is worth noting that a J_{sc} of 21% and 17% improvement was obtained for spray-processed TQ1:$PC_{61}BM$ and TQ1:$PC_{71}BM$ device with the substrate temperature of 75 °C compared to those spin-coated at 25 °C, respectively. This is mainly due to the efficient light harvesting and trapping for spray-coated devices as discussed in Section 3.3. To further confirm the accuracy of the *J*–*V* measurements in Fig. 8c, the corresponding EQE curves of the IFISCs were also measured, as shown in Fig. 8d. All of the devices exhibit a broad photoresponse in the wavelength range from 300 to 800 nm. The maximum of the EQEs reaches 39% and 46% for spray-processed TQ1:$PC_{61}BM$ and TQ1:$PC_{71}BM$ device, while 34% and 40% for the corresponding spin-coated devices, respectively. The calculated J_{sc} based on EQE spectra are in good agreement with the measured current values within 5% error. These results indicate spray-processed non-halogenated solvent mixtures can be successfully used in ITO-free R2R compatible PSCs fabrication processing.

4. Conclusions

In summary, using spray-coating technique, conventional ITO-based and inverted ITO-free PSCs were successfully fabricated. We provide a detailed investigation on multiple affecting factors of the spray-coating process, such as the solvents, solvent drying rates and thermal treatment. It is worth noting that the substrate temperatures and drying rates of the active layer enable to modulate the nano/micro-scale morphology and optimize charge transport properties in the spray-coated PSCs. Using the halogenated *o*DCB, the performance of the spray-coated PSCs approaches to that of the spin-coated devices. Notably, using the non-halogenated solvent mixtures TL:ID (80:20, v/v), the spray-coated PSC at 75 °C attains a superior PCE of 3.3%, which is even higher than that from the spin-coated devices using the same solvent. The enhanced J_{sc} stems from more light trapping in the textured microstructure and effective exciton dissociation in the blend films. In addition, the spray-coated IFISCs using this non-halogenated solvent mixtures were fabricated for the first time, where the spray-coated and spin-coated IFISCs show comparable device performance. It demonstrates that spray-coating method using non-halogenated solvents is a promising technique for environment-friendly PSC fabrication, presenting a bright future for the commercialization of spray-processed large-scale PSCs.

Acknowledgments

The authors are grateful to the NSFC project (#61274062 & #11204106) and the Open Fund of the State Key Laboratory of Luminescent Materials and Devices (South China University of Technology #2012-skllmd-10) and the Fundamental Research Funds for the Central Universities for the financial support. E. Wang acknowledges the Swedish Research Council Formas (VR) for the financial support.

Appendix A. Supporting information

Supplementary data associated with this article can be found in the online version at doi:10.1016/j.solmat.2016.11.027.

References

[1] N. Espinosa, M. Hösel, D. Angmo, F.C. Krebs, Solar cells with one-day energy payback for the factories of the future, Energy Environ. Sci. 5 (2012) 5117–5132.
[2] F.C. Krebs, N. Espinosa, M. Hösel, R.R. Søndergaard, M. Jørgensen, 25th anniversary article: rise to power - OPV-based solar parks, Adv. Mater. 26 (2014) 29–39.
[3] R. Søndergaard, M. Hösel, D. Angmo, T.T. Larsen-Olsen, F.C. Krebs, Roll-to-roll fabrication of polymer solar cells, Mater. Today 15 (2012) 36–49.
[4] G. Li, R. Zhu, Y. Yang, Polymer solar cells, Nat. Photonics 6 (2012) 153–161.
[5] J. Zhao, Y. Li, G. Yang, K. Jiang, H. Lin, H. Ade, W. Ma, H. Yan, Efficient organic solar cells processed from hydrocarbon solvents, Nat. Energy 1 (2016) 15027.
[6] W. Zhao, D. Qian, S. Zhang, S. Li, O. Inganas, F. Gao, J. Hou, Fullerene-free polymer solar cells with over 11% efficiency and excellent thermal stability, Adv. Mater. 28 (2016) 4734–4739.
[7] H. Zhou, Y. Zhang, C.K. Mai, S.D. Collins, G.C. Bazan, T.Q. Nguyen, A.J. Heeger, Polymer homo-tandem solar cells with best efficiency of 11.3%, Adv. Mater. 27 (2015) 1767–1773.
[8] C.N. Hoth, P. Schilinsky, S.A. Choulis, S. Balasubramanian, C.J. Brabec, Solution-Processed Organic Photovoltaics, 2013, pp. 27–56
[9] C.N. Hoth, S.A. Choulis, P. Schilinsky, C.J. Brabec, High photovoltaic performance of inkjet printed polymer:fullerene blends, Adv. Mater. 19 (2007) 3973–3978.
[10] K. Xiong, L. Hou, M. Wu, Y. Huo, W. Mo, Y. Yuan, W. Xu, S. Sun, E. Wang, From spin coating to doctor blading A systematic study on the photovoltaic performance of an isoindigo-based polymer, Sol. Energy Mater. Sol. Cells 132 (2015) 252–259.
[11] S.E. Shaheen, R. Radspinner, N. Peyghambarian, G.E. Jabbour, Fabrication of bulk heterojunction plastic solar cells by screen printing, Appl. Phys. Lett. 79 (2001) 2996–2998.
[12] G. Susanna, L. Salamandra, T.M. Brown, A. Di Carlo, F. Brunetti, A. Reale, Airbrush spray-coating of polymer bulk-heterojunction solar cells, Sol. Energy Mater. Sol. Cells 95 (2011) 1775–1778.
[13] C. Jeffrey, G. Tait, D. Cheyns, M. Turbiez, B.P. Rand, P. Heremans, Ultrasonic spray coating of 6.5% efficient diketopyrrolopyrrole-based organic photovoltaics, IEEE J. Photovolt. 4 (2014) 1538–1544.
[14] S.Y. Park, Y.J. Kang, S. Lee, D.G. Kim, J.K. Kim, J.H. Kim, J.W. Kang, Spray-coated organic solar cells with large-area of 12.25 cm(2), Sol. Energy Mater. Sol. Cells 95 (2011) 852–855.
[15] M. Schmidt, A. Falco, M. Loch, P. Lugli, G. Scarpa, Spray coated indium-tin-oxide-free organic photodiodes with PEDOT:PSS anodes, AIP Adv. 4 (2014) 107132.
[16] C. Kästner, S. Rathgeber, D.A.M. Egbe, H. Hoppe, Improvement of photovoltaic performance by ternary blending of amorphous and semi-crystalline polymer analogues with PCBM, J. Mater. Chem. A 1 (2013) 3961–3969.
[17] R. Hansson, L.K.E. Ericsson, N.P. Holmes, J. Rysz, A. Opitz, M. Campoy-Quiles, E. Wang, M.G. Barr, A.L.D. Kilcoyne, X. Zhou, P. Dastoor, E. Moons, Vertical and lateral morphology effects on solar cell performance for a thiophene–quinoxaline copolymer:PC70BM blend, J. Mater. Chem. A 3 (2015) 6970–6979.
[18] Z. Wang, E. Wang, L. Tao, F. Zhang, M. Andersoon, O. Inganäs, Mixed solvents for reproducible photovoltaic bulk heterojunctions, J. Photonics Energy 1 (2011) 011122.
[19] B. Schmidt-Hansberg, M. Sanyal, N. Grossiord, Y. Galagan, M. Baunach, M.F.G. Klein, A. Colsmann, P. Scharfer, U. Lemmer, H. Dosch, J. Michels, E. Barrena, W. Schabel, Investigation of non-halogenated solvent mixtures for high throughput fabrication of polymer–fullerene solar cells, Sol. Energy Mater. Sol. Cells 96 (2012) 195–201.
[20] K.-S. Chen, H.-L. Yip, C.W. Schlenker, D.S. Ginger, A.K.Y. Jen, Halogen-free solvent processing for sustainable development of high efficiency organic solar cells, Org. Electron. 13 (2012) 2870–2878.
[21] C.-D. Park, T.A. Fleetham, J. Li, B.D. Vogt, High performance bulk-heterojunction organic solar cells fabricated with non-halogenated solvent processing, Org. Electron. 12 (2011) 1465–1470.
[22] G. Susanna, L. Salamandra, C. Ciceroni, F. Mura, T.M. Brown, A. Reale, M. Rossi, A. Di Carlo, F. Brunetti, 8.7% Power conversion efficiency polymer solar cell realized with non-chlorinated solvents, Sol. Energy Mater. Sol. Cells 134 (2015) 194–198.
[23] Y. Kim, H.R. Yeom, J.Y. Kim, C. Yang, High-efficiency polymer solar cells with a cost-effective quinoxaline polymer through nanoscale morphology control induced by practical processing additives, Energy Environ. Sci. 6 (2013) 1909–1916.
[24] E. Wang, L. Hou, Z. Wang, S. Hellstrom, F. Zhang, O. Inganas, M.R. Andersson, An easily synthesized blue polymer for high-performance polymer solar cells, Adv. Mater. 22 (2010) 5240–5244.
[25] P. Kumar, S. Kannappan, P.-K. Shin, S. Ochiai, High-performance organic solar cells based on a low-bandgap poly-thienothiophene-benzodithiophene polymer and fullerene composite prepared by using the airbrush spray-coating technique, J. Korean Phys. Soc. 62 (2013) 1169–1175.
[26] D.J. Vak, S.S. Kim, J. Jo, S.H. Oh, S.I. Na, J.W. Kim, D.Y. Kim, Fabrication of organic bulk heterojunction solar cells by a spray deposition method for low-cost power generation, Appl. Phys. Lett. 91 (2007) 081102.
[27] M. Noebels, R.E. Cross, D.A. Evans, C.E. Finlayson, Characterization of spray-coating methods for conjugated polymer blend thin films, J. Mater. Sci. 49 (2014) 4279–4287.
[28] Y. Jang, J. Jo, D.-S. Kim, Control of doctor-blade coated poly (3,4-ethylenedioxythiophene)/poly(styrenesulfonate) electrodes shape on prepatterned substrates via microflow control in a drying droplet, J. Polym. Sci. B: Polym. Phys. 49 (2011) 1590–1596.
[29] A.C. Arias, N. Corcoran, M. Banach, R.H. Friend, J.D. MacKenzie, W.T.S. Huck, Vertically segregated polymer-blend photovoltaic thin-film structures through surface-mediated solution processing, Appl. Phys. Lett. 80 (2002) 1695–1697.
[30] M. Campoy-Quiles, T. Ferenczi, T. Agostinelli, P.G. Etchegoin, Y. Kim, T.D. Anthopoulos, P.N. Stavrinou, D.D. Bradley, J. Nelson, Morphology evolution via self-organization and lateral and vertical diffusion in polymer: fullerene solar cell blends, Nat. Mater. 7 (2008) 158–164.
[31] F. Aziz, A.F. Ismail, M. Aziz, T. Soga, Effect of solvent annealing on the crystallinity of spray coated ternary blend films prepared using low boiling point solvents, Chem. Eng. Process. 79 (2014) 48–55.
[32] J.-h. Lee, T. Sagawa, S. Yoshikawa, Morphological and topographical characterizations in spray coated organic solar cells using an additional solvent spray deposition, Org. Electron. 12 (2011) 2165–2173.
[33] C. Sprau, F. Buss, M. Wagner, D. Landerer, M. Koppitz, A. Schulz, D. Bahro, W. Schabel, P. Scharfer, A. Colsmann, Highly efficient polymer solar cells cast from non-halogenated xylene/anisaldehyde solution, Energ. Environ. Sci. 8 (2015) 2744–2752.
[34] S. Hong, M. Yi, H. Kang, J. Kong, W. Lee, J.-R. Kim, K. Lee, Effect of solvent on large-area polymer–fullerene solar cells fabricated by a slot-die coating method, Sol. Energy Mater. Sol. Cells 126 (2014) 107–112.
[35] Y. Zheng, R. Wu, W. Shi, Z. Guan, J. Yu, Effect of in situ annealing on the performance of spray coated polymer solar cells, Sol. Energy Mater. Sol. Cells 111 (2013) 200–205.
[36] H. Wu, B. Zhao, W. Wang, Z. Guo, W. Wei, Z. An, C. Gao, H. Chen, B. Xiao, Y. Xie, H. Wu, Y. Cao, Side chain modification: an effective approach to modulate the energy level of benzodithiophene based polymers for high-performance solar cells, J. Mater. Chem. A 3 (2015) 18115–18126.
[37] P. Robaeys, F. Bonaccorso, E. Bourgeois, J. D'Haen, W. Dierckx, W. Dexters, D. Spoltore, J. Drijkoningen, J. Liesenborgs, A. Lombardo, A.C. Ferrari, F. Van Reeth, K. Haenen, J.V. Manca, M. Nesladek, Enhanced performance of polymer:-fullerene bulk heterojunction solar cells upon graphene addition, Appl. Phys. Lett. 105 (2014) 083306.
[38] J. Miao, H. Chen, F. Liu, B. Zhao, L. Hu, Z. He, H. Wu, Efficiency enhancement in solution-processed organic small molecule: fullerene solar cells via solvent vapor annealing, Appl. Phys. Lett. 106 (2015) 183302.
[39] A. Maurano, C.C. Shuttle, R. Hamilton, A.M. Ballantyne, J. Nelson, W.M. Zhang, M. Heeney, J.R. Durrant, Transient optoelectronic analysis of charge carrier losses in a selenophene/fullerene blend solar cell, J. Phys. Chem. C 115 (2011) 5947–5957.
[40] T. Heumueller, W.R. Mateker, I.T. Sachs-Quintana, K. Vandewal, J.A. Bartelt, T.M. Burke, T. Ameri, C.J. Brabec, M.D. McGehee, Reducing burn-in voltage loss in polymer solar cells by increasing the polymer crystallinity, Energy Environ. Sci. 7 (2014) 2974–2980.
[41] P.W.M. Blom, V.D. Mihailetchi, L.J.A. Koster, D.E. Markov, Device physics of polymer:fullerene bulk heterojunction solar cells, Adv. Mater. 19 (2007) 1551–1566.
[42] H.-Y. Park, K. Kim, D.Y. Kim, S.-K. Choi, S.M. Jo, S.-Y. Jang, Facile external treatment for efficient nanoscale morphology control of polymer solar cells using a gas-assisted spray method, J. Mater. Chem. 21 (2011) 4457–4464.
[43] J.-S. Kim, W.-S. Chung, K. Kim, D.Y. Kim, K.-J. Paeng, S.M. Jo, S.-Y. Jang, Performance optimization of polymer solar cells using electrostatically sprayed photoactive layers, Adv. Funct. Mater. 20 (2010) 3538–3546.